Optical Imaging and Phototherapy

Subjects: Materials Science, Biomaterials

Contributor: Indrajit ROY

Theranostics is a key hallmark of cancer nanomedicine since it allows diagnosis and therapy of both primary and metastatic cancer using a single nanoprobe.

Keywords: theranostic nanoparticles ; image-guided therapy ; real-time therapy monitoring

1. Introduction

Over the past several years, the concept of theranostic nanoparticles, i.e., a single nanoprobe containing at least one diagnostic and one therapeutic functionality, has gained widespread attention [1][2]. Such nanoparticles offer two attractive biomedical benefits, namely, image-guided therapy and real-time therapy monitoring [3][4]. Several nanoparticles have shown promise for a new generation of imaging probes, with enhanced diagnostic features rather than traditional molecular imaging probes. Image-guided therapies involve, first, the acquisition of information about the precise anatomical location and/or the physiological condition of the diseased organ/tissue using high-resolution imaging. This is then followed by guided therapies that target the diseased site with precise spatio-temporal accuracy, thus causing a potent localized therapy without affecting normal organs/tissues. The progression of therapy can then be continuously monitored using the same imaging setup used during the original diagnosis. All these procedures can be carried out within a compact laboratory/clinical set-up, as shown schematically in **Figure 1**.

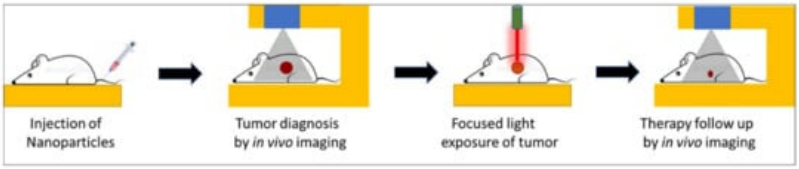

Figure 1. Schematic representation of key steps involved in image-guided light-activated therapy and subsequent therapy monitoring in a compact setting, beginning with a single injection of a tumor-bearing mouse with a theranostic nanoparticle.

Such lucrative biomedical possibilities are encouraged by the concurrent developments in diagnostic imaging technologies over the past few decades. These imaging modalities include magnetic resonance imaging (MRI), photoacoustic imaging (PAI), near-infrared fluorescence (NIRF) imaging, radio imaging techniques, such as positron emission tomography (PET), single-photon emission computed tomography (SPECT), X-ray computed tomography (CT) imaging, etc. Nanoparticles can serve as efficient imaging probes themselves, and/or can incorporate conventional diagnostic payload/s. Multifunctional nanoparticles offer the attractive possibility of targeted, image-guided therapy using a single nanoprobe with both diagnostic and therapeutic functions [5][6][7][8]. These functions can be inherent to the nanoparticle, owing to their novel physical properties at the nanoscale, or can be incorporated via physical/chemical means [9].

Light-activated therapies, such as photodynamic therapy (PDT) and photothermal therapy (PTT), are emerging as potent therapeutic interventions [10][11]. These therapies rely on the production of toxic species and/or heating upon the light-activation of photosensitive agents, called photosensitizers, via myriad mechanisms [12]. Several molecular photosensitizers serve as agents for PDT, whereby, upon light-activation, they interact with molecular oxygen in their excited state, and produce cytotoxic singlet oxygen ($^1O_2$). Examples of such photosensitizers include chlorins, pyropheophorbides, phthalocyanines, photofrin, etc. [13][14]. Some other photosensitizer molecules, upon light activation, generate reactive oxygen species (ROS), such as free radicals and/or heating via oxygen-independent mechanisms [15]. A few inorganic nanoparticles, such as titanium dioxide, also behave as photosensitizers for PDT as they produce $^1O_2$ and other ROS upon light activation [16]. Finally, the unique optical absorption properties of several nanostructures such as gold, carbon, etc., facilitates heat generation upon light activation. They serve as agents for PTT [17][18]. In addition to the

development of a variety of efficient photosensitizers, the advancement of photoactivated therapies is also aided by the refinement of light sources, such as lasers and light-emitting diodes (LEDs), for biomedical use [9]. The discovery of novel optical phenomena, such as aggregation-enhanced emission (AEE), multiphoton emission, photon upconversion, and Cerenkov luminescence, has further bolstered light-activated biomedical applications [19][20][21][22].

Evidently, the success of such therapies would critically hinge on the precise spatio-temporal accuracy of light activation on a fixed biological target for a limited time period. This is only possible with advanced imaging, which not only provides the precise anatomical location of the target but also the suitable time window that coincides with maximum drug accumulation at the target. A biocompatible, theranostic nanoparticle would be ideally suited to serve as the probe that would facilitate imaging and light-activated therapy in a compact medical set-up [9]. The nanoparticle itself can serve as a potent diagnostic probe, as well as acting as a photosensitizer. They also act as carriers of external diagnostic probes and/or molecular photosensitizers. A light-activated theranostic nanoformulation can be developed by combining at least one diagnostic probe and one photosensitizer [23][24][25]. Using state-of-the-art knowledge about the design and synthesis of nanoparticles, a multifunctional nanocomposite can be fabricated to contain multiple and independent active payloads, without compromising its overall physiological stability and biocompatibility. This review focuses on the use of such multifunctional theranostic nanoformulations in not only image-guided light-activated therapies but also real-time therapy monitoring. The subsequent sections are divided, based on the combination of a key imaging modality with phototherapy applications involving various theranostic nanoformulations. The scope of this review is presented in **Figure 2**. Owing to the vast literature already available in this area, we are unable to cover all such work in this review, and have cited only representative examples. We have also focused only on the in vivo phototheranostic applications of these nanoformulations.

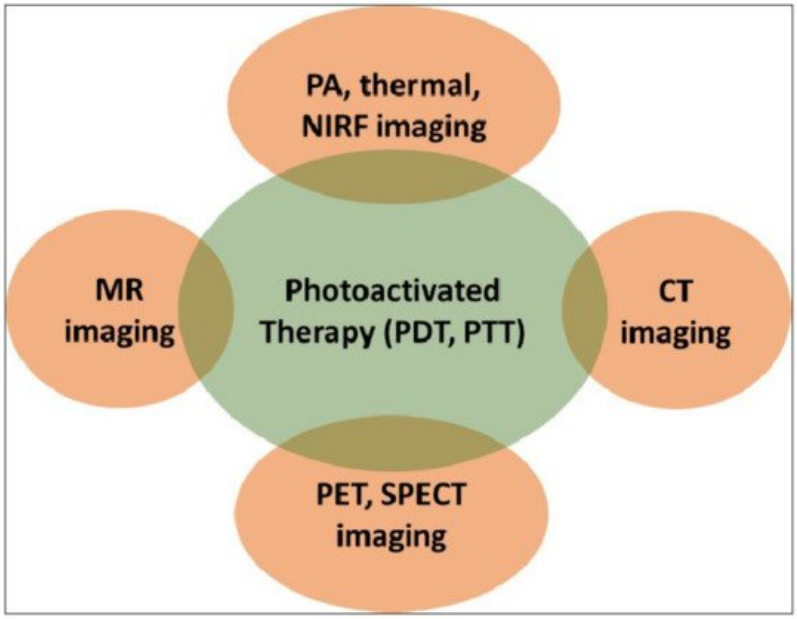

Figure 2. Schematic representation of the scope of this review. PDT—photodynamic therapy; PTT—photothermal therapy; MR—magnetic resonance; PA—photoacoustic; NIRF—near-infrared fluorescence; CT—computed tomography; PET—positron emission tomography; SPECT—single-photon emission computed tomography.

2. Optical Imaging and Phototherapy

A nanotheranostic formulation combining optical bioimaging and photoactivated therapy is quite simple to fabricate, as the same molecule or nanoparticle can have both an optical diagnostic and a phototherapeutic function [9]. For example, most photosensitizer molecules are weakly fluorescent and, thus, can facilitate both fluorescence bioimaging and PDT [14]. On the other hand, plasmonic nanostructures, such as gold nanorods, serve as dual probes for photoacoustic imaging (PAI) and PTT [18]. However, optical bioimaging can be significantly improved by introducing more efficient optical probes, such as upconversion nanoparticles (UCNPs), which convert incident light of lower energy to emitted light of higher energy [21]. UCNPs also aid in the indirect light activation of shorter wavelength-absorbing photosensitizers, using deep-penetrating long-wavelength incident light. Some of these examples are enlisted below.

2.1. Theranostic Gold Nanostructures

The nanoparticles of noble metals such as gold exhibit the property of localized surface plasmon resonance (SPR), in which the free electrons on their surface (plasmons) collectively oscillate upon exposure to light, resulting in strong plasmonic absorption bands. This physical phenomenon makes them suitable for several attractive biomedical applications, such as SPR-based sensing, photoacoustic tomographic (PAT) imaging, photothermal therapy, etc. [26][27].

Spherical gold nanoparticles (GNPs) show a sharp plasmonic band around 520 nm; however, this wavelength region is not optimal in terms of the tissue penetration of light. In order to red-shift this SPR absorption band toward the higher tissue-penetrating near-infrared (NIR) region, several higher-order and anisotropic nanostructures of gold have been developed, which include gold nanorods, nanoshells, nanostars, nanocages, etc. [28]. The controlled self-assembly of gold nanoparticles is another way to shift their absorption bands toward the NIR region, as a result of plasmonic coupling between neighboring nanoparticles. These higher-order gold nanostructures have attracted particular research interest because of their several biomedical applications, triggered by the deep tissue-penetrating NIR light.

Plasmonic photothermal therapy (PTT), resulting from effectively harnessing light energy to generate heat, is one of the most attractive biomedical applications of gold nanostructures. Pioneering works by Naomi Halas at Rice University, and Mostafa El-Sayed at Georgia Tech, have paved the way for the photothermal therapeutic applications of gold nanostructures in the pre-clinical and clinical settings [29][30]. Discoveries of novel in vivo imaging modalities using these gold nanostructures, such as photoacoustic tomography (PAT), have further bolstered their theranostic potential. Moreover, gold nanostructures can be loaded with additional diagnostic and/or therapeutic molecules, such as photosensitizers, for multimodal diagnostics and/or combination therapies (e.g., synergistic PTT and PDT). Below, we provide some representative examples of gold nanostructures as used for in vivo theranostic applications.

In one of the early demonstrations of image-guided PTT, Lu et al. fabricated hollow gold nanospheres (HAuNS) for in vivo PAT-mediated tumor detection, and subsequent PTT of the detected tumors. The integrin-targeted HAuNS were intravenously injected in a mouse model with orthotopically implanted glioma tumors. After PAT imaging, NIR-light irradiation on the detected tumor resulted in about a 20 °C increase in the tumor temperature, leading to efficient tumor ablation. This image-guided NIR-activated PTT could significantly enhance the median survival of treated mice [31].

Combination with additional drugs/photosensitizers enhances the multimodality of gold nanostructures. In one such example, Lin et al. developed gold vesicles (GVs) using assembled individual gold nanoparticles, which showed intense NIR absorbance (650–800 nm) due to the plasmonic coupling of individual gold nanoparticles (**Figure 3**). Furthermore, the GVs were used for encapsulating the photosensitizer Chlorin e6 (Ce6). This multimodal nanoassembly (GV-Ce6) could be applied for trimodal in vivo imaging (NIR fluorescence, thermal, and photoacoustic) following intratumoral injections in mice bearing subcutaneous MDA-MB-435 tumors (**Figure 4**). Subsequent tumor irradiation with a single laser (wavelength 671 nm) resulted in synergistic bimodal photoactivated therapy (PTT and PDT), leading to complete tumor eradication [32]. In another example involving drug-loaded gold nanostructures, Lee et al. prepared doxorubicin-loaded PEGylated hollow gold nanoshells (Dox@PEG-HAuNS) for photoacoustic-image guided combined chemo-photothermal therapy. They have also used fluorescence optical imaging and photoacoustic imaging to demonstrate in real-time an in vivo doxorubicin release and NIR laser-induced tumor-temperature rise, respectively. After mice bearing 4T1 tumors were intratumorally injected with Dox@PEG-HAuNS, photoacoustic imaging (acquisition wavelength = 800 nm) showed that laser treatment had resulted in a tumor temperature of 50 °C. The subsequent photothermal therapy was confirmed by histological analysis, demonstrating about double the tumor necrosis in mice treated with nanoparticles and laser than that in the non-laser treated control [33].

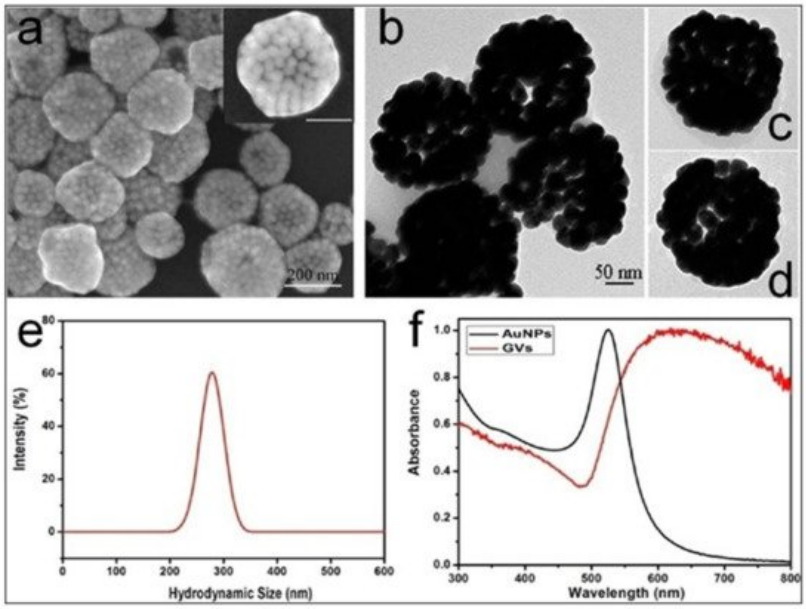

Figure 3. (**a**) Scanning electron microscopy (SEM), and (**b**–**d**) transmission electron microscopy (TEM) images of gold vesicles (GVs), showing the self-assembly (controlled clustering) of individual gold nanoparticles. (**e**) Dynamic light scattering (DLS) data showing the hydrodynamic size distribution of GVs. (**f**) UV—visible absorption spectra of individual gold nanoparticles (AuNPs) and GVs, showing that the sharp plasmonic peak of AuNPs around 520 nm shifts towards the red–NIR region (with substantial peak broadening) upon the formation of self-assembled GVs. Reproduced with permission from [32].

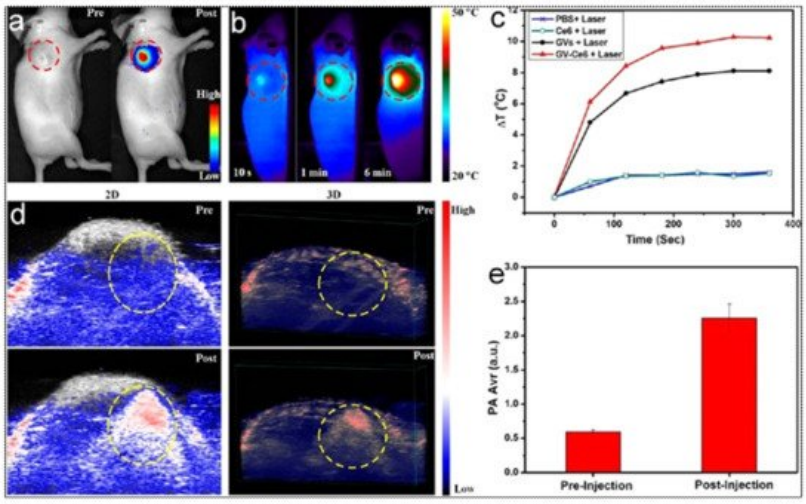

Figure 4. (**a**) In vivo whole-body NIRF image showing a substantial signal from tumors after post-injection of Ce6-loaded GVs (GV-Ce6), indicating the tumor accumulation of nanoparticles. The control image before (pre-) injection did not show any tumor-associated fluorescence. Tumors are indicated by dashed (red) circles. (**b**) Time-dependent thermal images of nanoparticle-accumulated tumors after exposure to 671 nm laser (2.0 W/cm2), for 6 min, following the treatment of mice with GV-Ce6, as well as various controls (PBS, Ce6 only, GVs only). Photo-thermal heating is seen only with the nanoformulations (GVs and GV-Ce6). (**c**) Heating curves of tumors upon laser irradiation as a function of irradiation time. (**d**) In vivo 2D and 3D photoacoustic (PA) images of tumors (indicated by yellow circles), and (**e**) average PA intensity of tumor, before (pre-injection) and after (post-injection) with GV-Ce6. A high PA signal enhance-ment is observed in the tumors post-injection with GV-Ce6. Reproduced with permission from [32].

Several reports have mentioned the use of self-assembled gold nanostructures with a plasmonic coupling-mediated intense optical signal in the NIR range for theranostic applications. Deng et al. devised amphiphilic mixed polymers grafted with controlled gold assemblies (GAs), showing a drastic plasmonic absorption shift from 520 nm to 830 nm [34]. These GAs showed a robust NIR photothermal conversion ability. Concurrently, owing to the high X-ray absorption coefficient of nanosized gold, these GAs were used in X-ray computed tomography (CT) imaging in mice bearing subcutaneous MCF-7 tumors. In vivo thermal imaging was also carried out to measure the enhancement of tumor temperature following the intratumoral injection of the GAs and activation using an 808 nm laser (power of 1 W/cm^2). A similar self-assembly of gold nanoparticles could also be triggered using heat, as shown by Sun et al., who used a thermally sensitive elastin-like polypeptide (ELP) conjugated on gold nanoparticles. These thermally responsive gold

nanoassemblies were applied in a scenario with NIR-light-triggered simultaneous photothermal/photoacoustic/X-ray CT imaging and photothermal therapy in a mouse model of melanoma, receiving a single intratumoral injection [35]. In a recent report, Zhang et al. have shown the use of acid-triggered aggregation of peptide-conjugated gold nanoparticles for multimodal (CT, photoacoustic, and photothermal) image-guided PTT in vivo [36].

2.2. Theranostic Carbon Nanostructures

Even since the discovery of carbon nanotubes (CNTs), various carbon nanostructures with unique optoelectronic properties are actively investigated for novel biomedical applications. Several of these nanostructures, such as CNTs, fullerenes, graphenes, carbon dots (CDs), and nanodiamonds, have received much attention in biomolecular imaging and therapy in the past few decades [37][38][39]. Some of these nanostructures show intense fluorescence for optical bioimaging, while others act as photosensitizers by generating reactive oxygen species (ROS) and/or heating upon light exposure [40]. Like gold nanostructures, the optical properties of carbon nanostructures can also be tuned in the deep tissue-penetrating NIR region. They can also be loaded with additional active diagnostic and/or therapeutic agents for multimodal image-guided therapy applications. Some of the representative examples of photo-theranostic carbon nanostructures are provided below.

Krishna et al. were the first to demonstrate water-soluble polyhydroxy fullerene (PHF) encapsulated in chitosan nanoparticles as an excellent PA and PTT in a mice model inoculated with BT474 breast cancer cells. A prominent photoacoustic contrast and significant tumor shrinkage (≈72%) was achieved at a single dose by the intratumor administration of the nanoparticles, followed by laser irradiation (785 nm, 500 mW, 10 min) [41].

Graphene Quantum dots (GQDs), which are disks of graphene in the size range of 2–20 nm, are an efficient PDT agent by overcoming the drawbacks of traditional porphyrin-based organic PDT agents, in terms of water-dispersibility, photostability, limited $^1O_2$ quantum yield ($\Phi < 1$) and inorganic semiconductor-based QDs regarding cytotoxicity or low-singlet oxygen generation. The integration of GQDs with a PDT agent for simultaneous imaging and PDT effects has been reported. However, Ge et al. have demonstrated the first example of red-emitting GQDs (2–6 nm), which can serve as a simultaneous imaging and PDT agent (λ_{ex} ≈680 nm). with exceptionally high $^1O_2$ yield ($\Phi \approx 1.3$) in mice with subcutaneous breast cancer xenografts. The high $^1O_2$ yield of GQDs (twice as high as that of the state-of-the-art PDT agent) is considered to stem from a new $^1O_2$-generating mechanism (multistate sensitization) [42].

Since the complete removal of the tumor either by PTT or PDT alone is challenging because of the absorption and scattering of photons in biological tissues, the combination of either of these therapies with chemotherapy, with an improved therapeutic response. has lately attracted extensive attention. Zhang et al. designed degradable hollow mesoporous silicon/carbon (Si/C) NPs as a carrier for a 31 wt % of the chemotherapeutic drug doxorubicin (DOX) for PA-imaging guided chemo-PTT in A549 tumor-bearing mice under laser irradiation (808 nm, 10 min, 1 W/cm^2). The strong PA (**Figure 5**) and thermal signals (≈50 °C), at the tumor site, along with a complete tumor reduction, confirmed its superior combinational chemo-PTT treatment, in contrast to uni-modal treatments [43].

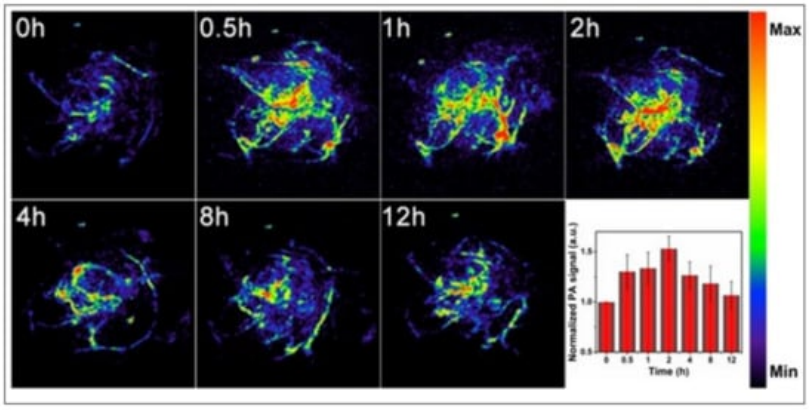

Figure 5. In vivo PA imaging of tumors, before (0 h) and after (0.5, 1, 2, 4, 8 and 12 h) intravenous injection of doxorubicin-containing hollow mesoporous Si/C nanoparticles, under 808-nm laser activation. Maximum tumor accumulation is observed 2 h post-injection. Inset shows time-dependent normalized PA signals in the tumor tissue. Reproduced with permission from [43].

Among the recently developed carbon nanostructures, carbon nanodots (CDs), also known as carbon quantum dots (<10 nm), have gained particular attention due to their effectiveness and versatility for cancer treatment. They differ from GO as they are spherical carbon particles with a size of less than 10 nm. They have aroused intense interest in bioimaging

because of their tunable photoluminescence, robust chemical inertness, and the presence of several surface carboxylic acid moieties, which provoke excellent water solubility, easy surface functionalization, and non-toxic nature, in contrast to traditional heavy-metal ion-based QDs. Wang et al. synthesized highly crystalline novel carbon nanodots (HCCDs) of 6–8 nm size for bimodal NIRF/PA imaging-guided PTT in U87 glioma-bearing mice. HCCDs not only exhibited strong long-wavelength NIR absorption (808 nm), owing to the larger extended π-electron system, but also a higher photothermal efficiency (η = 42.3%) as compared with GQDs (η = 28.6%). HCCDs have tunable fluorescence emissions and strong photoacoustic/photothermal efficiency [44].

Among graphene-based nanomaterials, GO nanosheets are an excellent PTT agent, combining the high drug loading of hydrophobic anticancer drugs or PS via π–π interactions. Recently, Hou et al. constructed a multifunctional nanotheranostic DiR-labelled HA-MTX prodrug-decorated GO nanosheet (≈200 nm) for NIRF-guided synergistic chemo-PTT in HeLa tumor-bearing BALB/c mice. The grafting of hyaluronic acid (HA) onto GO not only provided physiological stability and biocompatibility for prolonged blood circulation but also an active targeting affinity to tumor cells, with high expression of CD44 receptors. The results showed a strong fluorescence signal at the tumor tissue 12 and 24 h after injection, indicating the efficient tumor accumulation of the nanosystem via CD44 receptor-mediated active targeting [45].

2.3. Theranostic Upconversion Nanoparticles (UCNPs)

Upconversion nanophosphors (UCNPs) are inorganic nanomatrices, doped with trace amounts of certain rare-earth ions, which show the unique property of photon upconversion, where the sequential absorption of two low-energy (high-wavelength) photons leads to the emission of a high-energy (low-wavelength) photon [9][21]. By the controlled doping of rare-earth ions and adequate protection of UCNP surfaces, incident NIR light can be converted in various sharp emission bands spanning the UV and NIR region. As a result, UCNPs facilitate deep-tissue NIR-to-NIR optical bioimaging [46]. In addition, following NIR light activation, their emission bands can be exploited for the indirect activation of photosensitizers, including endogenous photosensitizers, such as riboflavin and Vitamin B2, in their vicinity through the energy-transfer mechanism [47][48]. Multimodal imaging and/or theranostics are possible using UCNPs co-doped with contrast agents for MR imaging (e.g., Gd), SPECT/PET imaging (e.g., radioactive isotopes), and therapeutic agents such as radionuclide, Yttrium-90, etc. [9][49]. Therefore, UCNPs play a critical role in optical bioimaging and photoactivated therapies that can be combined in a nanotheranostic platform. Some representative examples are provided below.

Tsai et al. synthesized oleic-acid-coated UCNPs, conjugated with the tumor-targeting peptide angiopep-2 (ANG), the photothermal agent IR-780, and the photosensitizer 5,10,15,20-tetrakis(3-hydroxyphenyl) chlorin (mTHPC). These hybrid UCNPs, termed ANG-INMPs, could successfully permeate across the blood–brain barrier and target orthotopic glioblastoma multiforme (GBM) tumors in the mouse brain, as revealed by live animal optical imaging using the IVIS instrument (**Figure 6**). Subsequent activation of the as-diagnosed tumors with an NIR laser (980/808 nm) resulted in robust combination phototherapy (PTT and PDT) in vivo, as ascertained by tumor immunohistochemistry (IHC) and Kaplan–Meier survival analysis. Tumor immunohistochemistry revealed significant apoptosis, as well as the necrosis of tumor cells receiving the targeted dual photo therapies [50].

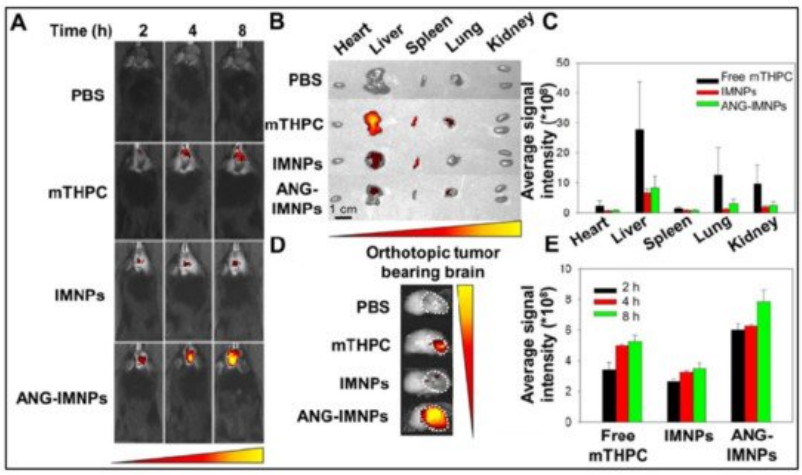

Figure 6. (**A**) Orthotopic glioma tumors in mice visualized by whole-body in vivo fluorescence imaging, following intravenous injection of PBS, free photosensitizer mTHPC, UCNPs containing dye IR-780 and mTHPC (IMNPs), and IMNPs conjugated with targeting peptide angiopep-2 (ANG-IMNPs). Maximum tumor accumulation can be observed in tumors treated with ANG-IMNPs. (**B**) Ex vivo fluorescence images of dissected major organs. No major off-target effect was seen except for liver and spleen accumulation of mice treated with free mTHPC. (**C**) Average fluorescence intensity of mTHPC in major organs, showing some liver, lung and kidney accumulation in mice treated with free mTHPC. (**D**) Ex

vivo fluorescence images, and (**E**) quantitative evaluation of tumor accumulation in the brain, showing the maximum tumor accumulation of ANG-IMNPs. Reproduced with permission from [50].

More complex UCNPs can be designed to enable orthogonal emission, in response to excitation by two different lasers. For example, Tang et al. developed photoswitching upconversion nanoparticles (UCNPs) showing orthogonal emissive behavior, whereby red and green emission is obtained upon excitation by 980 nm and 808 nm lasers, respectively. In a mouse model bearing A-549 lung tumors, the authors demonstrated that the green emission can be used as an imaging signal to diagnose and monitor the tumor, whereas the red emission can be used to excite the conjugated photosensitizer zinc phthalocyanine (ZnPc) for NIR-activated PDT [51]. Similar photo-switchable upconversion nanoparticles were also prepared by Zuo et al. that prominently emit in the red wavelength (660 nm) upon 800 nm light excitation, and in the UV-blue range upon 980 nm excitation. The former is used for optical diagnostics, whereas the latter is used for triggering PDT [52].

2.4. Theranostic 2D Nanostructures

Several two-dimensional (2D) inorganic-based nanostructures are increasingly being used in biomedical applications, owing to their unique optoelectronic properties, as well as the ease of surface functionalization for enhanced hydrophilicity, biocompatibility, and incorporation of additional active agents [53]. In these nanostructures, the third dimension is atomically thin, i.e., consisting of just a few layers of atoms. Black phosphorous (BP), bismuth-based nanosheets, and MXenes are some examples of such exciting nanostructures; we shall provide some representative examples of the theranostic applications of these nanostructures in this section.

In an early example, Sun et al. reported the high-energy mechanical milling-mediated preparation of water-soluble and PEGylated BP nanostructures, which showed high photostability and the ability for NIR-light activated photothermal therapy in vitro. They are also suitable agents for photoacoustic (PA) imaging, as evidenced by a PA imaging mediated demonstration of their high tumor accumulation via passive targeting following systemic administration, in mice bearing subcutaneous 4T1 breast tumors. Subsequent exposure of NIR light (808 nm diode laser, with a power density of 1.0 W/cm^2) to the as-diagnosed tumors led to robust tumor ablation and the near-complete recovery of the tumor-bearing mice. No toxic side effect was observed in the treated mice, highlighting the biocompatibility of these nanoparticles. This result shows that a single theranostic nanoprobe with both diagnostic and therapeutic functions can be used for efficient photoactivated cancer therapy [54]. Other active agents can also be incorporated within BP nanoparticles for multimodal theranostic applications. In a recent report, Huang et al. incorporated aggregation-induced emission (AIE)-active photosensitizers with BP for dual-modal (NIR fluorescence and photothermal) imaging-guided combined PDT and PTT application. The prepared AIE photosensitizer TTPy-incorporated BP nanosheets showed excellent NIR emission, photostability, biocompatibility, and photoactivated generation of both localized heating and $^1O_2$. Following systemic administration in mice bearing 4T1 tumors, efficient tumor accumulation could be visualized by NIR fluorescence and photoactivated thermal imaging. The as-diagnosed tumors were then exposed to either NIR laser light (808 nm, power density of 1.0 W/cm^2), or white light (100 mW/cm^2), or both. Complete tumor eradication with no tumor recurrence was observed for the tumors exposed to both NIR and white light, because of synergistic photothermal and photodynamic therapies, whereas PTT alone (NIR-light exposure only) and PDT alone (white light exposure only) led to only partial tumor ablation. This report shows the benefits of combination therapies using multimodal theranostic nanomaterials, based on the BP platform [55].

Bismuth-based nanosheets, such as those of Bi_2Te_3, show a strong absorbance in the NIR region and high photothermal conversion efficiency; thus, they can be used for optical theranostic applications. Bai et al. incorporated the photosensitizer methylene blue (MB) with bovine serum albumin (BSA)-coated Bi_2Te_3 nanosheets for bimodal PTT/PDT combination therapy. The highly photostable and biocompatible BSA–Bi_2Te_3/MB nanoparticles could demonstrate both photothermal (activated by 808 nm laser, power density 1.0 W/cm^2) and photodynamic (activated by 650 nm laser, power density 50 mW/cm^2) therapeutic effects in a mouse model bearing U14 squamous cell carcinoma tumors, leading to complete tumor elimination [56]. Wang et al. constructed nanotheranostic Bi_2Se_3/$MoSe_2$/ Bi_2Se_3 sandwich heterostructures with the incorporated drug doxorubicin for multimodal (CT and photothermal) image-guided photoactivated combination cancer therapy. Herein, first, ultrasound-mediated exfoliation led to the formation of $MoSe_2$ nanosheets (5–30 nm), followed by cation exchange-mediated generation of the sandwich nano heterostructures, with a narrow bandgap (1.17 eV), and robust NIR absorption with high photothermal conversion efficiency (59.3%). The high X-ray absorption coefficient of Bi led to high CT-imaging contrast for the detection of U-14 tumors in mice treated with these nano constructs. Tumor exposure of an NIR laser (808 nm, 1 W/cm^2) resulted in combined PDT and PTT, along with enhanced drug release for additional chemotherapy [57].

MXenes are another exciting class of inorganic-based 2D nanomaterials, which include transition-metal carbides, nitrides, and carbonitrides [58]. In a pioneering report, Lin et al. reported the fabrication of functional 2D tantalum carbide (Ta_4C_3 MXene) nanosheets, via the liquid-phase exfoliation of Ta_4AlC_3 ceramics. These 2D Ta_4C_3 nanosheets showed high photothermal-conversion efficiency (η of 44.7%) and served as agents for dual-modal photoacoustic and CT imaging in vivo, in mice bearing 4T1 breast tumors. NIR laser (808 nm, power density 1.5 W/cm^2) exposure of the tumors led to potent photothermal tumor ablation [59]. MXenes also provide a platform for the incorporation of other functional nanoparticles for multimodality. Han et al. prepared mesoporous silica-coated niobium carbide (Nb_2C) MXenes using sol-gel chemistry, with cetanecyltrimethylammonium chloride (CTAC) trapped within the mesopores for chemotherapy. The core Nb_2C MXenes showed excellent photothermal conversion efficiency (28.6%) in the NIR-II region (1000–1350 nm), where a high tissue penetration of light is observed. The MXenes were further PEGylated and conjugated with the cyclic arginine-glycine-aspartic pentapeptide c(RGDyC) for enhanced systemic circulation and tumor targeting. Photoacoustic imaging was used to demonstrate the efficient tumor targeting of the targeted MXene-based nanostructures in a mouse model with subcutaneous U87 neuroglioma xenografts. Tumor exposure to NIR-II laser light (1064 nm, 1.5 W/cm^2) resulted in very high tumor inhibition (inhibition efficiency: 92.37%) [60]. The above results amply demonstrate the potential of these 2D nanostructures to serve as ideal platforms for multimodal and efficient theranostic applications in the treatment of cancer and other diseases.

References

1. Baetke, S.C.; Lammers, T.; Kiessling, F. Applications of nanoparticles for diagnosis and therapy of cancer. Br. J. Radiol. 2015, 88, 20150207.
2. Chen, F.; Ehlerding, E.B.; Cai, W. Theranostic nanoparticles. J. Nucl. Med. 2014, 55, 1919–1922.
3. Terreno, E.; Uggeri, F.; Aime, S. Image guided therapy: The advent of theranostic agents. J. Cont. Rel. 2012, 161, 328–337.
4. Chen, F.; Hableel, G.; Zhao, E.R.; Jokerst, J.V. Multifunctional nanomedicine with silica: Role of silica in nanoparticles for theranostic, imaging, and drug monitoring. J. Colloid Interface Sci. 2018, 521, 261–279.
5. Burke, B.P.; Cawthorne, C.; Archibald, S.J. Multimodal nanoparticle imaging agents: Design and applications. Philos. Trans. R. Soc. 2017, 375, 20170261.
6. Cha, B.G.; Kim, J. Functional mesoporous silica nanoparticles for bio-imaging applications. Wiley Interdiscip. Rev. Nanomed. Nanobiotechnol. 2019, 11, e1515.
7. Key, J.; Leary, J.F. Nanoparticles for multimodal in vivo imaging in nanomedicine. Int. J. Nanomed. 2014, 9, 711–726.
8. Lee, D.E.; Koo, H.; Sun, I.C.; Ryu, J.H.; Kim, K.; Kwon, I.C. Multifunctional nanoparticles for multimodal imaging and theragnosis. Chem. Soc. Rev. 2012, 41, 2656–2672.
9. Chen, G.; Roy, I.; Yang, C.; Prasad, P.N. Nanochemistry and Nanomedicine for Nanoparticle-based Diagnostics and Therapy. Chem. Rev. 2016, 116, 2826–2885.
10. Dolmans, D.E.; Fukumura, D.; Jain, R.K. Photodynamic therapy for cancer. Nat. Rev. Cancer 2003, 3, 380–387.
11. Zhi, D.; Yang, T.; O'Hagan, J.; Zhang, S.; Donnelly, R.F. Photothermal therapy. J. Cont. Rel. 2020, 325, 52–71.
12. Hou, Y.J.; Yang, X.X.; Liu, R.Q.; Zhao, D.; Guo, C.X.; Zhu, A.C.; Wen, M.N.; Liu, Z.; Qu, G.F.; Meng, H.X. Pathological Mechanism of Photodynamic Therapy and Photothermal Therapy Based on Nanoparticles. Int. J. Nanomed. 2020, 15, 6827–6838.
13. Shi, X.; Zhang, C.Y.; Gao, J.; Wang, Z. Recent advances in photodynamic therapy for cancer and infectious diseases. Wiley Interdiscip. Rev. Nanomed. Nanobiotechnol. 2019, 11, e1560.
14. Abrahamse, H.; Hamblin, M.R. New photosensitizers for photodynamic therapy. Biochem. J. 2016, 473, 347–364.
15. Larue, L.; Myrzakhmetov, B.; Ben-Mihoub, A.; Moussaron, A.; Thomas, N.; Arnoux, P.; Baros, F.; Vanderesse, R.; Acherar, S.; Frochot, C. Fighting Hypoxia to Improve PDT. Pharmaceuticals 2019, 12, 163.
16. Çeşmeli, S.; Biray, A.C. Application of titanium dioxide (TiO(2)) nanoparticles in cancer therapies. J. Drug Target. 2019, 27, 762–766.
17. Liu, Y.; Bhattarai, P.; Dai, Z.; Chen, X. Photothermal therapy and photoacoustic imaging via nanotheranostics in fighting cancer. Chem. Soc. Rev. 2019, 48, 2053–2108.
18. Hou, X.; Tao, Y.; Pang, Y.; Li, X.; Jiang, G.; Liu, Y. Nanoparticle-based photothermal and photodynamic immunotherapy for tumor treatment. Int. J. Cancer 2018, 143, 3050–3060.

19. Hu, F.; Xu, S.; Liu, B. Photosensitizers with Aggregation-Induced Emission: Materials and Biomedical Applications. Adv. Mater. 2018, 30, e1801350.
20. Guo, L.; Wong, M.S. Multiphoton excited fluorescent materials for frequency upconversion emission and fluorescent probes. Adv. Mater. 2014, 26, 5400–5428.
21. Yang, D.; Li, C.; Lin, J. Multimodal cancer imaging using lanthanide-based upconversion nanoparticles. Nanomedicine 2015, 10, 2573–2591.
22. Das, S.; Thorek, D.L.; Grimm, J. Cerenkov imaging. Adv. Cancer Res. 2014, 124, 213–234.
23. Melancon, M.P.; Zhou, M.; Li, C. Cancer theranostics with near-infrared light-activatable multimodal nanoparticles. Acc. Chem. Res. 2011, 44, 947–956.
24. Chen, H.; Zhao, Y. Applications of Light-Responsive Systems for Cancer Theranostics. ACS Appl. Mater. Interfaces 2018, 10, 21021–21034.
25. Vankayala, R.; Hwang, K.C. Near-Infrared-Light-Activatable Nanomaterial-Mediated Phototheranostic Nanomedicines: An Emerging Paradigm for Cancer Treatment. Adv. Mater. 2018, 30, e1706320.
26. Cabuzu, D.; Cirja, A.; Puiu, R.; Grumezescu, A.M. Biomedical applications of gold nanoparticles. Curr. Top. Med. Chem. 2015, 15, 1605–1613.
27. Liu, Y.; Crawford, B.M.; Vo-Dinh, T. Gold nanoparticles-mediated photothermal therapy and immunotherapy. Immunotherapy 2018, 10, 1175–1188.
28. Kohout, C.; Santi, C.; Polito, L. Anisotropic Gold Nanoparticles in Biomedical Applications. Int. J. Mol. Sci. 2018, 19, 3385.
29. Lal, S.; Clare, S.E.; Halas, N.J. Nanoshell-enabled photothermal cancer therapy: Impending clinical impact. Acc. Chem. Res. 2008, 41, 1842–1851.
30. Huang, X.; El-Sayed, I.H.; Qian, W.; El-Sayed, M.A. Cancer cell imaging and photothermal therapy in the near-infrared region by using gold nanorods. J. Am. Chem. Soc. 2006, 128, 2115–2120.
31. Lu, W.; Melancon, M.P.; Xiong, C.; Huang, Q.; Elliott, A.; Song, S.; Zhang, R.; Flores 2nd, L.G.; Gelovani, J.G.; Wang, L.V.; et al. Effects of photoacoustic imaging and photothermal ablation therapy mediated by targeted hollow gold nanospheres in an orthotopic mouse xenograft model of glioma. Cancer Res. 2011, 71, 6116–6121.
32. Lin, J.; Wang, S.; Huang, P.; Wang, Z.; Chen, S.; Niu, G.; Li, W.; He, J.; Cui, D.; Lu, G.; et al. Photosensitizer-loaded gold vesicles with strong plasmonic coupling effect for imaging-guided photothermal/photodynamic therapy. ACS Nano 2013, 7, 5320–5329.
33. Lee, H.J.; Liu, Y.; Zhao, J.; Zhou, M.; Bouchard, R.B.; Mitcham, T.; Wallace, M.; Stafford, J.; Li, C.; Gupta, S.; et al. In Vitro and in vivo mapping of drug release after laser ablation thermal therapy with doxorubicin-loaded hollow gold nanoshells using fluorescence and photoacoustic imaging. J. Cont. Rel. 2013, 172, 152–158.
34. Deng, H.; Zhong, Y.; Du, M.; Liu, Q.; Fan, Z.; Dai, F.; Zhang, X. Theranostic self-assembly structure of gold nanoparticles for NIR photothermal therapy and X-ray computed tomography imaging. Theranostics 2014, 4, 904–918.
35. Sun, M.; Peng, D.; Hao, H.; Hu, J.; Wang, D.; Wang, K.; Liu, J.; Guo, X.; Wei, Y.; Gao, W. Thermally Triggered in Situ Assembly of Gold Nanoparticles for Cancer Multimodal Imaging and Photothermal Therapy. ACS Appl. Mater. Interfaces 2017, 9, 10453–10460.
36. Zhang, Y.; Chang, J.; Huang, F.; Yang, L.; Ren, C.; Ma, L.; Zhang, W.; Dong, H.; Liu, J.; Liu, J. Acid-Triggered in Situ Aggregation of Gold Nanoparticles for Multimodal Tumor Imaging and Photothermal Therapy. ACS Biomater. Sci. Eng. 2019, 5, 1589–1601.
37. Sharma, P.; Mehra, N.K.; Jain, K.; Jain, N.K. Biomedical Applications of Carbon Nanotubes: A Critical Review. Curr. Drug Deliv. 2016, 13, 796–817.
38. Liao, C.; Li, Y.; Tjong, S.C. Graphene Nanomaterials: Synthesis, Biocompatibility, and Cytotoxicity. Int. J. Mol. Sci. 2018, 19, 3564.
39. Mohajeri, M.; Behnam, B.; Sahebkar, A. Biomedical applications of carbon nanomaterials: Drug and gene delivery potentials. J. Cell Physiol. 2018, 234, 298–319.
40. Jiang, B.P.; Zhou, B.; Lin, Z.; Liang, H.; Shen, X.C. Recent Advances in Carbon Nanomaterials for Cancer Phototherapy. Chemistry 2019, 25, 3993–4004.
41. Krishna, V.; Singh, A.; Sharma, P.; Iwakuma, N.; Wang, Q.; Zhang, Q.; Knapik, J.; Jiang, H.; Grobmyer, S.R.; Koopman, B.; et al. Polyhydroxy fullerenes for non-invasive cancer imaging and therapy. Small 2010, 6, 2236–2241.

42. Ge, J.; Lan, M.; Zhou, B.; Liu, W.; Guo, L.; Wang, H.; Jia, Q.; Niu, G.; Huang, X.; Zhou, H.; et al. A graphene quantum dot photodynamic therapy agent with high singlet oxygen generation. Nat. Commun. 2014, 5, 4596.
43. Zhang, J.; Zhang, J.; Li, W.; Chen, R.; Zhang, Z.; Zhang, W.; Tang, Y.; Chen, X.; Liu, G.; Lee, C.S. Degradable hollow mesoporous silicon/carbon nanoparticles for photoacoustic imaging-guided highly effective chemo-thermal tumor therapy in vitro and in vivo. Theranostics 2017, 7, 3007–3020.
44. Qian, M.; Du, Y.; Wang, S.; Li, C.; Jiang, H.; Shi, W.; Chen, J.; Wang, Y.; Wagner, E.; Huang, R. Highly Crystalline Multicolor Carbon Nanodots for Dual-Modal Imaging-Guided Photothermal Therapy of Glioma. ACS Appl. Mater. Interfaces 2018, 10, 4031–4040.
45. Zhang, H.; Li, Y.; Pan, Z.; Chen, Y.; Fan, Z.; Tian, H.; Zhou, S.; Zhang, Y.; Shang, J.; Jiang, B.; et al. Multifunctional Nanosystem Based on Graphene Oxide for Synergistic Multistage Tumor-Targeting and Combined Chemo-Photothermal Therapy. Mol. Pharm. 2019, 16, 1982–1998.
46. Chen, G.; Yang, C.; Prasad, P.N. Nanophotonics and nanochemistry: Controlling the excitation dynamics for frequency up- and down-conversion in lanthanide-doped nanoparticles. Acc. Chem. Res. 2013, 46, 1474–1786.
47. Qiu, H.; Tan, M.; Ohulchanskyy, T.Y.; Lovell, J.F.; Chen, G. Recent Progress in Upconversion Photodynamic Therapy. Nanomaterials 2018, 8, 344.
48. Khaydukov, E.V.; Mironova, K.E.; Semchishen, V.A.; Generalova, A.N.; Nechaev, A.V.; Khochenkov, D.A.; Stepanova, E.V.; Lebedev, O.I.; Zvyagin, A.V.; Deyev, S.M.; et al. Riboflavin photoactivation by upconversion nanoparticles for cancer treatment. Sci. Rep. 2016, 6, 35103.
49. Guryev, E.L.; Volodina, N.O.; Shilyagina, N.Y.; Gudkov, S.V.; Balalaeva, I.V.; Volovetskiy, A.B.; Lyubeshkin, A.V.; Sen', A.V.; Ermilov, S.A.; Vodeneev, V.A.; et al. Radioactive (90Y) upconversion nanoparticles conjugated with recombinant targeted toxin for synergistic nanotheranostics of cancer. Proc. Natl. Acad. Sci. USA 2018, 115, 9690–9695.
50. Tsai, Y.C.; Vijayaraghavan, P.; Chiang, W.H.; Chen, H.H.; Liu, T.I.; Shen, M.Y.; Omoto, A.; Kamimura, M.; Soga, K.; Chiu, H.C. Targeted Delivery of Functionalized Upconversion Nanoparticles for Externally Triggered Photothermal/Photodynamic Therapies of Brain Glioblastoma. Theranostics 2018, 8, 1435–1448.
51. Tang, M.; Zhu, X.; Zhang, Y.; Zhang, Z.; Zhang, Z.; Mei, Q.; Zhang, J.; Wu, M.; Liu, J.; Zhang, Y. Near-Infrared Excited Orthogonal Emissive Upconversion Nanoparticles for Imaging-Guided On-Demand Therapy. ACS Nano 2019, 13, 10405–10418.
52. Zuo, J.; Tu, L.; Li, Q.; Feng, Y.; Que, I.; Zhang, Y.; Liu, X.; Xue, B.; Cruz, L.J.; Chang, Y.; et al. Near Infrared Light Sensitive Ultraviolet-Blue Nanophotoswitch for Imaging-Guided "Off-On" Therapy. ACS Nano 2018, 12, 3217–3225.
53. Cheng, L.; Wang, X.; Gong, F.; Liu, T.; Liu, Z. 2D Nanomaterials for Cancer Theranostic Applications. Adv. Mater. 2020, 32, 1902333.
54. Sun, C.; Wen, L.; Zeng, J.; Wang, Y.; Sun, Q.; Deng, L.; Zhao, C.; Li, Z. One-pot solventless preparation of PEGylated black phosphorus nanoparticles for photoacoustic imaging and photothermal therapy of cancer. Biomaterials 2016, 91, 81–89.
55. Huang, J.; He, B.; Zhang, Z.; Li, Y.; Kang, M.; Wang, Y.; Li, K.; Wang, D.; Tang, B.Z. Aggregation-Induced Emission Luminogens Married to 2D Black Phosphorus Nanosheets for Highly Efficient Multimodal Theranostics. Adv. Mater. 2020, 32, 2003382.
56. Bai, J.; Jia, X.; Ruan, Y.; Wang, C.; Jiang, Z. Photosensitizer-Conjugated Bi2Te3 Nanosheets as Theranostic Agent for Synergistic Photothermal and Photodynamic Therapy. Inorg. Chem. 2018, 57, 10180–10188.
57. Wang, Y.; Zhao, J.; Chen, Z.; Zhang, F.; Wang, Q.; Guo, W.; Wang, K.; Lin, H.; Qu, F. Construct of MoSe2/Bi2Se3 nanoheterostructure: Multimodal CT/PT imaging-guided PTT/PDT/chemotherapy for cancer treating. Biomaterials 2019, 217, 119282.
58. Lin, H.; Chen, Y.; Shi, J. Insights into 2D MXenes for Versatile Biomedical Applications: Current Advances and Challenges Ahead. Adv. Sci. 2018, 5, 1800518.
59. Lin, H.; Wang, Y.; Gao, S.; Chen, Y.; Shi, J. Theranostic 2D Tantalum Carbide (MXene). Adv. Mater. 2017, 30, 1703284.
60. Han, X.; Jing, X.; Yang, D.; Lin, H.; Wang, Z.; Ran, H.; Li, P. Therapeutic mesopore construction on 2D Nb2C MXenes for targeted and enhanced chemo-photothermal cancer therapy in NIR-II biowindow. Theranostics 2018, 8, 4491–4508.